Pressure separation and gas flows in a prototype vacuum-pumped solar-thermochemical reactor

Ivan Ermanoski, Adrian Orozco, and Johannes Grobbel

Citation: AIP Conference Proceedings **1850**, 100004 (2017); doi: 10.1063/1.4984461
View online: http://dx.doi.org/10.1063/1.4984461
View Table of Contents: http://aip.scitation.org/toc/apc/1850/1
Published by the American Institute of Physics

Pressure Separation and Gas Flows in a Prototype Vacuum-Pumped Solar-Thermochemical Reactor

Ivan Ermanoski[1, a)], Adrian Orozco[1], and Johannes Grobbel[2]

[1]*Sandia National Laboratories, PO Box 5800, MS 1415, Albuquerque, NM 87123, USA*
[2]*German Aerospace Center, Professor-Rehm-Straße 1, 52428 Jülich, Germany*

[a)]Corresponding author: iermano@sandia.gov

Abstract. A detailed design of pressure separation by packed columns of particles, in a solar-thermochemical reactor prototype, is presented. Results show that the concept is sound and robust under a multitude operational conditions. Straightforward control approaches, such as pumping speed and pressure adjustments, can be implemented to cover a wide range of contingencies.

INTRODUCTION

Two-step thermochemical cycles are a theoretically efficient and a conceptually simple solar fuel production approach. In the high temperature step—thermal reduction—a reactive material (oxide) is partially or fully reduced. In low temperature step—oxidation—the reduced oxide is exposed to steam or CO_2, to produce H_2 or CO. At practical temperatures, the thermal reduction step requires vacuum pumping or inert gas sweeping to lower the local oxygen pressure—both presenting their own challenges.[1-7]

A cascading pumping approach, using multiple reduction stages at successively lower pressures, has been predicted to achieve a tenfold pressure decrease compared to a single-stage design.[8] To demonstrate the cascading reactor concept, as well particle-based continuous H_2 production cycle at realistic process temperatures and pressures, we have designed a prototype device with two thermal reduction chambers (TRCs), targeting p_{TR1}~100Pa and p_{TR2}~30Pa, and identical volumetric pumping speeds (Fig. 1). A custom solar simulator will deliver a total of ~3kW at the apertures. The design is compatible with oxides in particle form, and will initially work with CeO_2.

The feasibility of pressure separation in a particle bed has been examined in some of our previous works, at a conceptual level.[9] However, an engineering solution for a reactor prototype demands a more rigorous analysis.

METHODS AND RESULTS

Design Requirements, Goals and Limitations

Packed bed pressure separation enables vacuum reduction and avoids two types of recombination losses. First, H_2–O_2 recombination via H_2 flow from the water splitting chamber (WSC) to the TRC; and second, $CeO_{2-\delta}$-O_2 oxidation, via O_2 flow from the TRCs (~1450°C) to the cooler segments. With good design, these losses can be neglected in efficiency calculations [10, 11]. To fulfill these roles, *the particle beds in the reactor must not fluidize*.

Pressure separation on the one hand, and particle flow in the reactor and gas flow in the WSC on the other, have opposing requirements. Small particles (i.e. low bed permeability) in narrow and long interconnecting segments, give the best pressure separation. Conversely, reliable particle flow throughout the system, and a countercurrent steam-particle flow in the WSC, suggest wide tubes (to avoid interlocking arches) and large particles (to avoid cohesive arches, and WSC fluidization by minimizing the Δp along it). Finally, segment lengths are vertically limited, so substantial design optimization is needed.

SolarPACES 2016
AIP Conf. Proc. 1850, 100004-1–100004-8; doi: 10.1063/1.4984461
Published by AIP Publishing. 978-0-7354-1522-5/$30.00

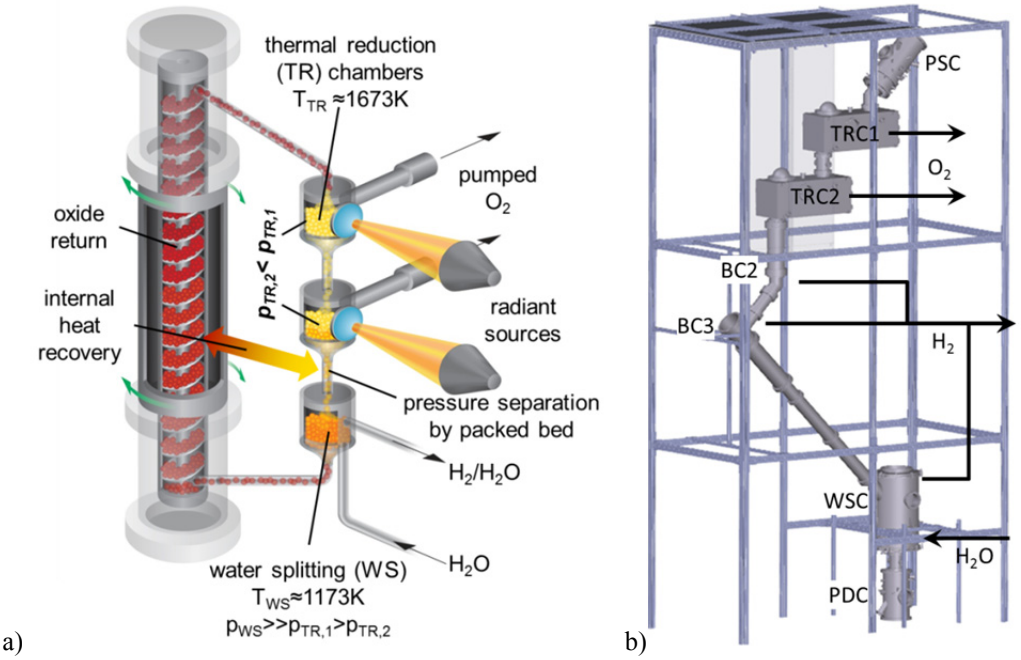

FIGURE 1. (a) Cascading pressure reactor concept; (b) Schematic of a ~7m tall prototype, with two TRCs, a support structure outline, and indicated gas flows. The oxide flows to TRC1 from the particle source chamber (PSC), and is reduced in TRC1 and TRC2. In the WSC, the oxide is exposed to steam, to produce H_2. The oxide then flows into a particle drain chamber (PDC), and is returned to the PSC (return not shown). Pressure separation requires "buffer" chambers—BC3 (10kPa) and BC2 (800Pa). Pressures (except p_{WS}) are controlled via corresponding pumping speeds.

Modeling Approach

A column of particles must satisfy two conditions to remain packed under opposing gas pressure. First, it must not be lifted ("blown") by the gas from below—i.e. the downward pressure of particles above any z-position, must be higher than the Δp between z and the top of the bed: $p_{bed}(z) > p(z) - p(z_{top})$. Second, the gas velocity at the bed top must be lower than the particles' terminal (settling) velocity—else gas flow can carry them away individually.

Pressure as function of vertical position in the bed, $p(z)$, is calculated using the Ergun equation with a Knudsen correction factor $f_c(Kn)$, to account for different flow regimes (viscous and molecular, depending on pressure):

$$\frac{\mathrm{d}p(z)}{\mathrm{d}z} = -\frac{\dot{m}_g}{A(z)}\frac{RT}{p(z)MD_p}\frac{1-\phi}{\phi^3}\left[\frac{150(1-\phi)\mu}{f_c\,(Kn)D_p} + 1.75\frac{\dot{m}_g}{A(z)}\right] \qquad (1).$$

Here, $\dot{m}_g$ is the gas mass flow through the bed, $A(z)$ is the bed cross-section area, M is the gas molar mass, D_p is the particle diameter, ϕ is the bed void fraction, μ is the gas dynamic viscosity, and T is the temperature. The Knudsen correction factor $f_c(Kn)$ depends on pressure and is calculated as follows:

$$f_c = [1 + \alpha(Kn)Kn]\left[1 + \frac{4Kn}{1-bKn}\right], \text{ where} \qquad Kn = \frac{\lambda}{D_p} \qquad \text{and} \qquad \lambda = \frac{k_B T}{\sqrt{2}\pi d^2 p} \qquad (2)\text{a, b, c.}$$

Here, Kn is the Knudsen number, λ is the gas mean free path, d is the molecular diameter (d_{H2}=0.297nm, d_{H2O}=0.275nm). Steam and H_2 viscosities are calculated from the works of Stiel and Thodos, and Sengers and Kamgar-Parsi.[12, 13] The coefficient b=-1 is used for slip flow (large Kn), and $\alpha(Kn)$ is calculated as follows:

$$\alpha(Kn) = \alpha_0 \frac{2}{\pi} tan^{-1}\left(\alpha_1 Kn^{\beta}\right), \qquad \text{where } \alpha_0 \equiv \alpha_{Kn\to\infty} = \frac{64}{3\pi\left(1-\frac{4}{b}\right)} \qquad \text{and} \qquad \beta = 0.4 \qquad (3)\text{a, b, c.}$$

To apply Eq.(1), several initial assumptions were made. (1) the bed is near-stationary, (2) the net particle exchange between the gas and the solid is negligible (ceria cycles between CeO_2 and $CeO_{1.96}$), (3) bed temperature is uniform, (4) all particles have the same D_p, (4) the void fraction is uniform across the bed, and (5) the problem can be treated 1-dimensionally, along the flow direction.

Particle terminal velocity (v_t) is calculated from Stokes' law, with a Cunningham correction for slip flow:[14-18]

$$v_t = \frac{C(\rho_{solid}-\rho_{gas})D_p}{18} \quad \text{where} \quad C = 1 + A \cdot Kn \quad \text{and} \quad A = \alpha + \beta e^{\frac{-\gamma}{Kn}} \quad (4)\text{a, b, c}$$

The coefficient A depends weakly on the specific gas and solid combinations[15, 19], so the same α, β, γ coefficients (for oil in air) were used for all gasses in our system (CeO_2 in H_2, O_2, and steam).

Results and Discussion

Pressure Separation Above the Water Splitting Chamber

The analysis and results are focused on the most challenging segment—separation between WSC and TRC2, where Δp~1atm (requiring a tall bed) and p_{WS}/p_{TR}~1000. Steam and H_2 flows are examined separately. To determine $p(z)$, and $p(l)$ for non-vertical beds, Equation (1) is solved numerically under baseline assumptions: D_p=300μm, ϕ=0.4, bed height H=2.2m, (L=3.1m, at 45°), p_{WS}=82.8kPa—the Albuquerqe ambient pressure. Superficial velocity, v_s, in the ullage space equals the actual gas flow velocity, relevant for the lift of individual particles at the top.

Preliminary designs Some designs, such as the examples in Fig. 2, had no practical solutions. Figure 2a, shows results for WSC→TRC H_2 flow (p_{TR}=100Pa), through a constant bed diameter d_b=15mm. The bed fluidizes above l~0.7m, where $p(l)>p_{max}$—the maximum "hydrostatic" pressure the bed weight can sustain.

In Fig. 2b, abrupt v_s drops indicate d_b increases, introduced to keep $p(l)$ below $0.9p_{max}$ in the entire bed, and to maintain a net-downwards force for particle flow. Fluidization is prevented, but d_{b5}=200mm—impractical with standard vacuum components. Moreover, at the design CeO_2 flow rate $\dot{m}_{CeO2}$≈2g/s, the anticipated H_2 production rate is $\dot{m}_{H2,prod}$~400μg/s. At a H_2 mass flow rate $\dot{m}_{H2}$=600μg/s, H_2 is completely lost to H_2-O_2 recombination in the TRC—one of the issues to be prevented by pressure separation. The volumetric flow $\dot{V}_{H2,RT}$—given at ambient temperature (27°C) and indicating the TRC pumping speed needed to maintain p_{TR}—is also large, and exceeds the TRC O_2 pumping speed.

These examples reveal the need for intermediate chambers (BC3 and BC2 in Fig. 1b).

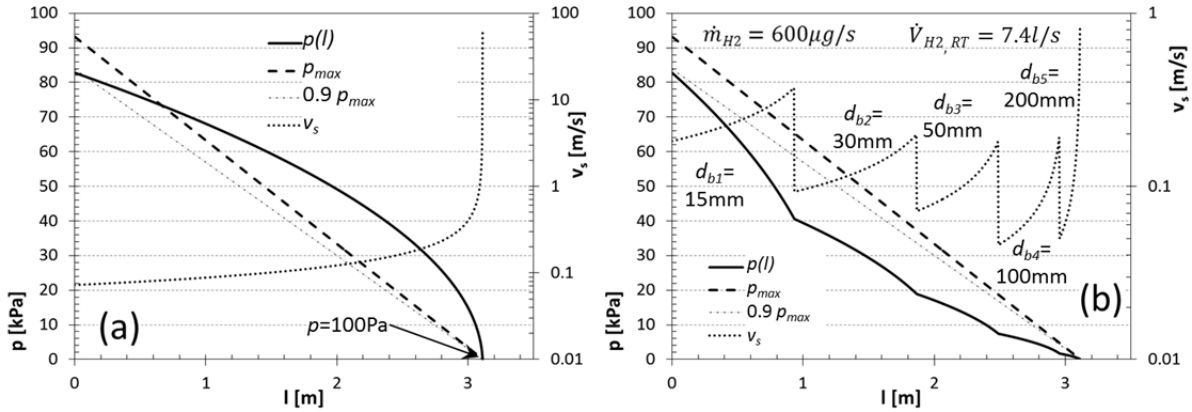

FIGURE 2. Pressure and v_s profiles for direct WSC-TRC H_2 flow. Solid black lines are $p(l)$, dashed lines are p_{max}, and the thin dash-dot lines are 90% of p_{max}. The dotted line (right-hand axis) is v_s. (a) Constant d_b (b) Expanding d_b.

Baseline case The results for a baseline WSC→BC3 H_2 flow are shown in Fig. 3a, where d_b increases from d_{b1}=15mm to d_{b5}=100mm. Fluidization is prevented, and because p_{BC3}=10kPa>>p_{TR}=100Pa, $\dot{V}_{H2,RT}$=43ml/s is much smaller than in Fig. 2b (7.4l/s), and is easily pumped. The flow at 800°C ($\dot{V}_{H2,800}$)—i.e. at the bed top—is 154ml/s. At the pump outlet, this flow is ~5.2ml/s. Even though $\dot{m}_{H2}$=345μg/s is comparable to $\dot{m}_{H2,prod}$~400μg/s, the gasses from BC3 are pumped to the common H_2 output line, so no recombination takes place and no H_2 is lost (Fig. 1b). As

a contingency, the WSC is designed for operation down to ~10kPa, limited by oxidation kinetics and WSC steam flow constraints.

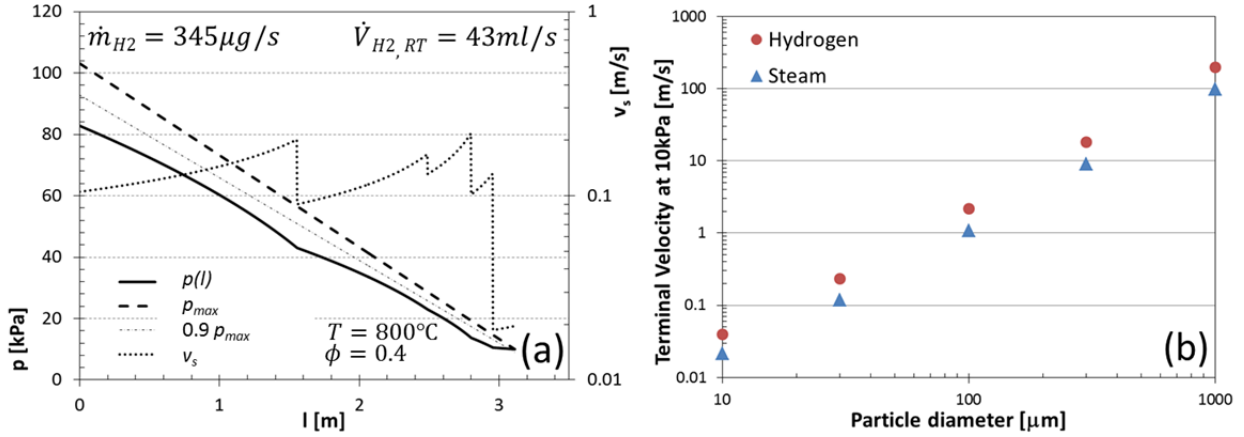

FIGURE 3. (a) Pressure and v_s profiles for a baseline WSC-BC3 H_2 flow. (b) Terminal velocity (v_t) of spherical ceria particles in H_2 and steam, at 10kPa and 800°C.

The last diameter increase—at the top of the bed—serves to decrease v_s, to minimize the lifting of fine particles inevitably present in the system. For particles of nominal size (D_p=300μm), $v_t >> v_s$ at the top of the bed (Fig. 3a,b), so they cannot be lifted. Only particles with D_p<20μm experience sufficient lift to be carried away from the top.

The v_s results support the stationary bed approximation: From the density of ceria, ρ=7.2g/cm^3, follows a bulk density $\rho_{bulk}=\rho\phi$=4.32g/cm^3, and a flow velocity in the narrowest section, v_{CeO2}=2.6mm/s—much smaller than the corresponding H_2 flow velocity v_s≈150mm/s.

The oxide moving slowly through the reactor, a smaller d_b could be considered a better design solution. Our experiments indicate that d_b=15mm is near the limit of flow feasibility under the variety of anticipated conditions, so operation would be risked by using narrower beds. Nonetheless, in a larger and better characterized device, higher length to diameter ratios would be feasible and advantageous.

Gas composition Before exploring the variety of possible conditions arising in operation, such as void fraction, temperature, particle size, etc., the baseline case for steam flow in the WSC-BC3 segment is also examined (Fig. 4). This situation corresponds to a WSC steam feed rate far in excess of the minimum needed for reoxidation.

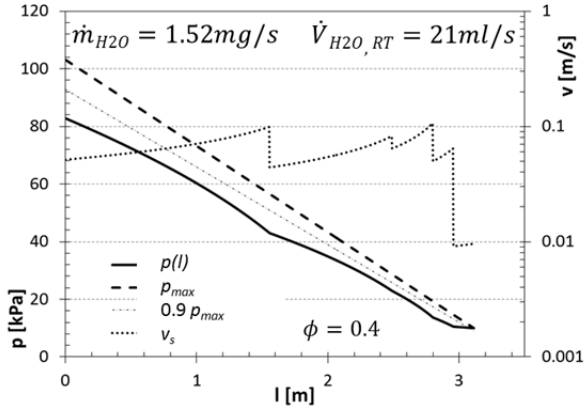

FIGURE 4. Pressure and v_s profiles for a baseline WSC-BC3 H_2O (steam) flow case, with conditions same as in Fig. 3a.

Some important observations can be made about the results in Fig. 4. First, the pressure profile for steam is identical to that for H_2. This somewhat intuitive result sets aside any concerns that fluidization could occur owing to a varying H_2/H_2O ratio in the WSC or along the bed. Second, v_s is roughly half of that for the H_2 case, and in line with the ratio of terminal velocities (Fig. 3b), thus allaying concerns regarding particle lift at the top of the bed. The only substantial difference between H_2 and steam—a higher mass flow, owing to the higher molecular mass of water

compared to H_2—is of negligible experimental and operational consequence. The remainder of the presented analysis therefore focuses on H_2.

Effect of void fraction While ϕ~0.4 can be expected under the prototype operating conditions, the steep ϕ-dependence in Equation (1) warrants caution. The results for likely extremes of ϕ, corresponding to close random packing and loose random packing, are shown in Fig. 5.

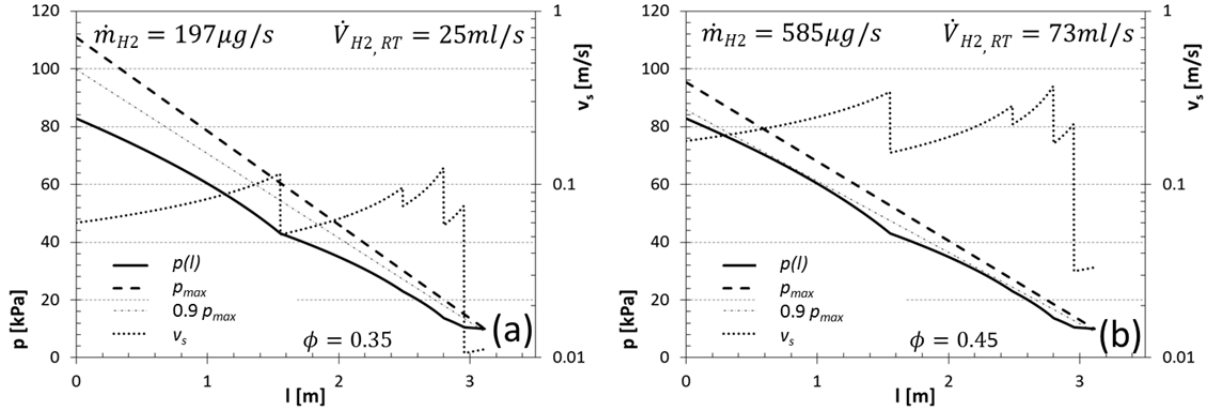

FIGURE 5. Pressure and v_s profiles for ϕ (a) below (ϕ=0.35), and (b) above (ϕ=0.45), the baseline (ϕ=0.4) in Fig. 3a.

The effects of varying ϕ are qualitatively intuitive: a lower ϕ (denser bed) gives a lower gas flow rate and higher margin between p and p_{max}, and *vice versa*. Importantly, the effects are relatively small, and do not bring into question the operation of the reactor, should the void fraction deviate from the baseline, or even if variations are present along the bed. Considering the low required pumping speeds, any feasible void fraction scenario can be managed by adjusting the pumping speed at BC3and, if necessary, p_{WS}.

Effect of particle size It is rather unlikely that particles will be narrowly distributed around the design size D_p=300μm. In fact, one of the larger unknowns about the operation of a reactor of this type, is the equilibrium particle size distribution, resulting from long-term operation, and determined by the competing effects of attrition and sintering. To gain some understanding on the effects of particle size, the baseline case is examined for two additional sizes—D_p=100μm, and D_p=500μm (i.e. ±200μm from the design size). The results are shown in Fig. 6.

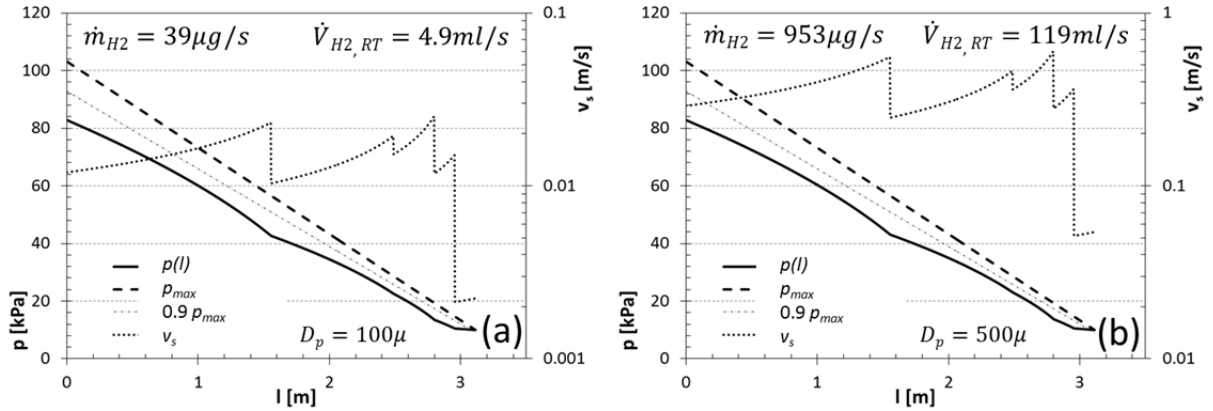

FIGURE 6. Pressure and v_s profiles for particle sizes (a) below (D_p=100μm), and (b) above (D_p=500μm), the baseline in Fig. 3a. Note the different v_s scale between the plots.

Qualitatively, the results are in line with expectations: smaller particles lower the gas flow, owing to a lower permeability. Quantitatively, it is very encouraging that D_p=100μm particles greatly diminish gas flow, yielding a roughly order of magnitude difference from the 300μm particles. On the other end, flow for D_p=500μm particles is just under three times higher than the baseline. Much like previous cases, both situations can be managed by

adjusting the BC3 pumping speed and, if necessary, p_{WS}. The pressure profiles for both particle sizes are identical to the baseline, thus not jeopardizing the packed state of the bed, irrespective of the particle size distribution.

Even though particle size seems to be manageable in terms of gas flow, concerns remain with respect to particle flow, should the average diameter enter regimes of cohesive or interlocking arch formation. Without sufficient experience in operating a reactor, this must continue to be an open issue—one that can nonetheless be resolved by designing bed diameters appropriate for experimentally determined equilibrium particle sizes.

Effects of temperature The final factor under consideration is temperature dependence, evaluated below and above the baseline. Two competing effects play a role with temperature change. First, the viscosity of H_2 and steam (and gasses in general) increases with temperature, causing a permeation decrease. Second, gasses expand with temperature increase, increasing volumetric flow. The results in Fig. 7 show that temperature plays a minor role in pressure separation, with pressure profiles (again) identical to the baseline, and only minor differences in flow rates.

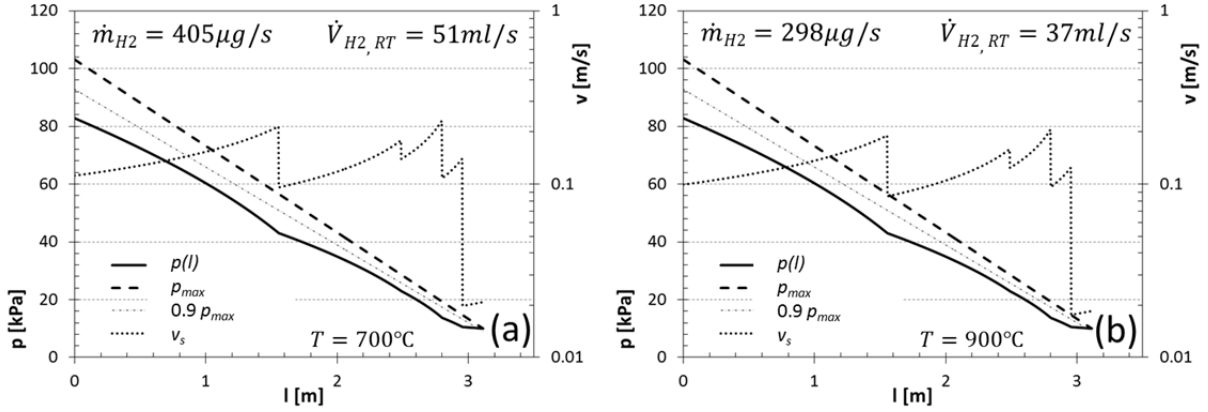

FIGURE 7. Pressure and v_s profiles for T (a) below (T=700°C), and (b) above (T=900°C), the baseline in Fig. 3a.

In summary, the above results show that pressure separation by a slowly moving packed particle bed is robust to changes in gas composition, void fraction, particle size distribution, and temperature. Changes can be managed by modestly adjusting the pumping speed at the top of the bed and, if necessary, the pressure at its bottom.

The next section, BC3-BC2, has differences and similarities with the WSC-BC3 section. The absolute pressure difference is lower by a factor of ~10, so the bed height needed for pressure separation is much smaller (35cm for BC3-BC2, vs. 2.2m for WSC-BC3). The pressure ratio is higher, so bed expansion is still necessary, and it drives bed height more than the pressure difference does. The need for expansion is mitigated by a decrease in v_t with decreasing pressure, allowing for higher superficial velocities at the top of the bed. A solution for this segment is shown in Fig. 8a, for the worst-case: ϕ=0.45, and T=800°C—lower density and temperature than anticipated.

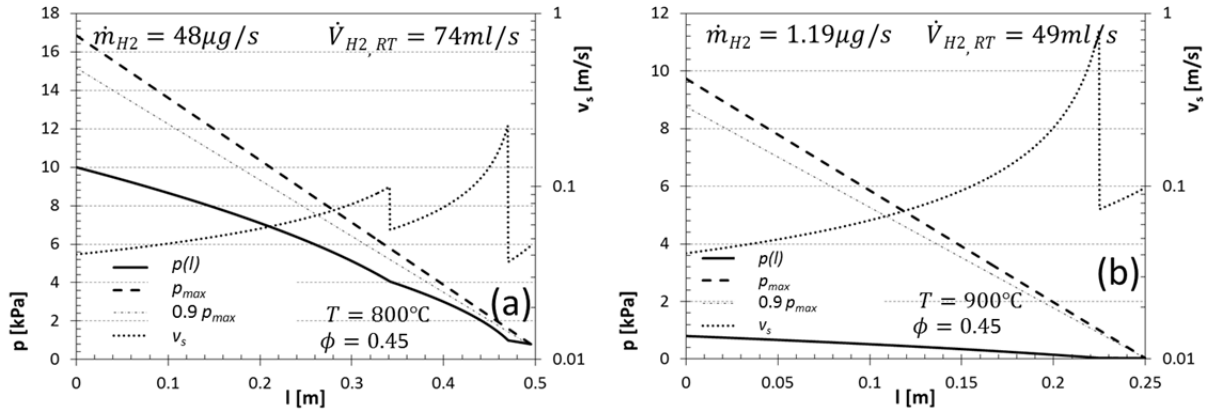

FIGURE 8. Pressure and v_s profiles in (a) the BC3-BC2, and (b) the BC2-TRC2 sections (p_{BC2}=800Pa, p_{TRC2}=30Pa, ϕ=0.45).

The results for the final segment, BC2-TRC2 are shown in Fig. 8b. Comparing $\dot{m}_{H2}$ between segments, a dramatic decrease is evident: from 345μg/s in the WSC-BC3 segment (Fig. 3), to at most 1.2μg/s predicted to reach TRC2 from BC2—assuming all of the gas permeating through the particle column is H_2, and none is steam. At $\dot{m}_{H2,prod}$~400μg/s, the resulting H_2-O_2 recombination loss, would be a negligible 0.3%—at most.

Pressure Separation Below the Thermal Reduction Chamber

An interesting problem arises in the segment(s) below TRC2. The reduced oxide in these segments is no longer exposed to a (simulated) solar flux, which inevitably leads to some cooling. If the surrounding gas is similar in composition and pressure to that in TRC2, i.e. O_2 at p_{TR}, such cooling would lead to the swift $CeO_{2-\delta}$-O_2 reoxidation, and a potentially significant loss of efficiency. To glean some understanding of the extent of the issue, the potential losses for three idealized cases are examined, assuming that reduced particles leave TRC2 through a 15mm tube, and that they do not substantially cool in the first 100mm, 50mm, and 10mm of downward motion. For the design ceria mass flow rate $\dot{m}_{CeO2}$≈2g/s ($\dot{n}_{CeO2}$≈11.6mmol/s) and v_{CeO2}=2.6mm/s, these distances correspond to 38s, 19s, and 3.8s of travel time.

The O_2 flow rate down to a given bed depth depends on the pressure difference $\Delta p=p_{TRC2}-p(z)$, but not the pressure ratio, so setting $p(z)$=0.1Pa, for example, is a satisfactory assumption, irrespective of the actual p_{O2} above the cooled reduced oxide. Calculated O_2 mass flow rates $\dot{m}_{O2}$ to the three bed depths are shown in Fig. 9.

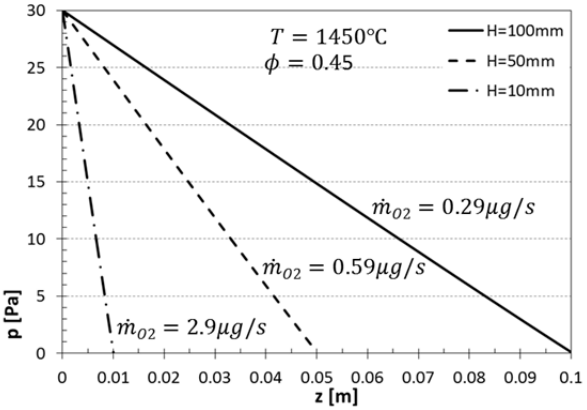

FIGURE 9. Oxygen pressure between TRC2 (p_{TRC2}=30Pa) and three depths in a d_b=15mm bed of 300μm particles.

The results in Fig. 9 need to be compared with the design O_2 production rate in TRC2. The extent of ceria reduction in TRC2 (at 30Pa), is δ_{TR2}=0.01761, and in TRC1 (at 100Pa), δ_{TR2}=0.01397, yielding $\Delta\delta$=0.00364 and $\dot{n}_{O2,TRC2}$=21.2μmol/s. the corresponding mass flow is $\dot{m}_{O2,TRC2}$=677μg/s—much larger than any of the values in Fig. 9. Evidently, an insignificant fraction of the oxygen from TRC2 would reach even the shallowest of the three bed depths, to very slightly reoxidize the ceria. Put simply, if reduced oxide particles are covered by as little as 1cm of bed, they are mostly "protected" from reoxidation if their temperature decreases.

It is important to appreciate that the above is the worst-case scenario, in which O_2 is assumed to permeate down through the bed unopposed. In practice, a small flow of H_2 and steam in the opposite direction would exist (Fig. 8b), and O_2 permeation from the TRCs toward BC2 would be much lower than the results Fig. 9. Moreover, other measures, such as a small inert gas purge below the TRCs, can further decrease $CeO_{2-\delta}$-O_2 oxidation.

CONCLUSIONS

A detailed engineering design of pressure separation by packed columns of particles, in a solar thermochemical reactor prototype, shows that the concept is sound and robust under a multitude of varying conditions that may be encountered in operation, such as gas composition, void fraction, particle size distribution, and temperature. Some design limitations on bed heights and diameters, which exist in a small prototype, would not be present in a MW-sized device, thus likely enabling a simpler and even more robust design, as well as an even lower impact of gas separation/permeation on efficiency.

ACKNOWLEDGEMENTS

This work is part of a project titled "High Efficiency Solar Thermochemical Reactor for Hydrogen Production", supported by the U.S. Department of Energy Fuel Cell Technologies Office. The authors gratefully acknowledge the contributions of our colleagues from Sandia National Laboratories, the German Aerospace Center, Bucknell University, and Arizona State University. Sandia is a multiprogram laboratory operated by Sandia Corporation, a Lockheed Martin Company, for the United States Department of Energy's National Nuclear Security Administration under Contract DE-AC04-94AL85000.

REFERENCES

1. T. Nakamura, Sol. Energy **19**, 467-475 (1977).
2. E. A. Fletcher and R. L. Moen, Science **197**, 1050-1056 (1977).
3. Y. Tamaura, A. Steinfeld, P. Kuhn, and K. Ehrensberger, Energy **20**, 325-330 (1995).
4. N. Gokon, S. Takahashi, H. Yamamoto, and T. Kodama, Int. J. Hydrogen Energy **33**, 2189-2199 (2008).
5. R. B. Diver, J. E. Miller, M. D. Allendorf, N. P. Siegel, and R. E. Hogan, J. Sol. Energy Eng. **130**, 041001-041001 -041001-041008 (2008).
6. J. Lapp, J. H. Davidson, and W. Lipinski, Energy **37**, 591-600 (2012).
7. I. Ermanoski, N. P. Siegel, and E. B. Stechel, J. Sol. Energy Eng. **135**, 031002-031001 - 031010 (2013).
8. I. Ermanoski, Int. J. Hydrogen Energy **39**, 13114-13117 (2014).
9. I. Ermanoski, et al., AIP Conference Proceedings **1734**, 120001 (2016).
10. I. Ermanoski, J. E. Miller, and M. D. Allendorf, PCCP **16**, 8418-8427 (2014).
11. I. Ermanoski, Energy Procedia **69**, 1731-1740 (2015).
12. L. I. Stiel and G. Thodos, Ind. Eng. Chem. Fundam. **2**, 233-& (1963).
13. J. V. Sengers and B. Kamgarparsi, J. Phys. Chem. Ref. Data **13**, 185-205 (1984).
14. E. Cunningham, Proc. R. soc. Lond. Ser. A-Contain. Pap. Math. Phys. Character **83**, 357-365 (1910).
15. Y. Ishida, Phys. Rev. **21**, 0550-0563 (1923).
16. M. Knudsen and S. Weber, Ann. Phys.-Berlin **36**, 983-996 (1911).
17. R. A. Millikan, Phys. Rev. **22**, 1-23 (1923).
18. R. A. Millikan, Phys. Rev. **21**, 217-238 (1923).
19. D. J. Rader, J. Aerosol. Sci. **21**, 161-168 (1990).